

See discussions, stats, and author profiles for this publication at: <https://www.researchgate.net/publication/223968087>

Noble Metal Coated Single-Walled Carbon Nanotubes for Applications in Surface Enhanced Raman Scattering Imaging and Photothermal Therapy

ARTICLE *in* JOURNAL OF THE AMERICAN CHEMICAL SOCIETY · APRIL 2012

Impact Factor: 12.11 · DOI: 10.1021/ja300140c · Source: PubMed

CITATIONS

135

READS

38

5 AUTHORS, INCLUDING:



Xiaojing Wang

University of California, Riverside

2 PUBLICATIONS 143 CITATIONS

[SEE PROFILE](#)



Liang Cheng

Suzhou University

116 PUBLICATIONS 3,933 CITATIONS

[SEE PROFILE](#)

Noble Metal Coated Single-Walled Carbon Nanotubes for Applications in Surface Enhanced Raman Scattering Imaging and Photothermal Therapy

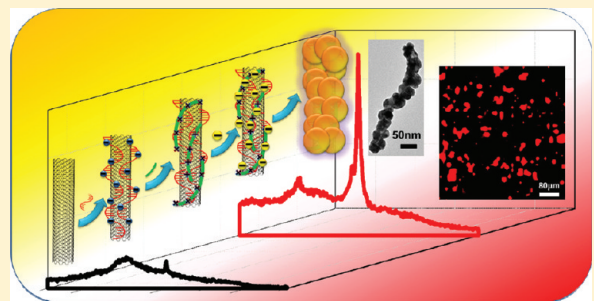
Xiaojing Wang,[†] Chao Wang,[†] Liang Cheng,[†] Shuit-Tong Lee,[‡] and Zhuang Liu^{*,†}

[†]Jiangsu Key Laboratory for Carbon-Based Functional Materials & Devices, Institute of Functional Nano & Soft Materials Laboratory (FUNSOM), Soochow University, Suzhou, Jiangsu 215123, China

[‡]Center of Super-Diamond and Advanced Films (COSDAF) and Department of Physics and Materials Science, City University of Hong Kong, Hong Kong SAR, China

Supporting Information

ABSTRACT: Single-walled carbon nanotubes (SWNTs) with various unique optical properties are interesting nanoprobes widely explored in biomedical imaging and phototherapies. Herein, DNA-functionalized SWNTs are modified with noble metal (Ag or Au) nanoparticles via an *in situ* solution phase synthesis method comprised of seed attachment, seeded growth, and surface modification with polyethylene glycol (PEG), yielding SWNT-Ag-PEG and SWNT-Au-PEG nanocomposites stable in physiological environments. With gold or silver nanoparticles decorated on the surface, the SWNT-metal nanocomposites gain an excellent concentration and excitation-source dependent surface-enhanced Raman scattering (SERS) effect. Using a near-infrared (NIR) laser as the excitation source, targeted Raman imaging of cancer cells labeled with folic acid (FA) conjugated SWNT-Au nanocomposite (SWNT-Au-PEG-FA) is realized, with images acquired in significantly shortened periods of time as compared to that of using nonenhanced SWNT Raman probes. Owing to the strong surface plasmon resonance absorption contributed by the gold shell, the SWNTs-Au-PEG-FA nanocomposite also offers remarkably improved photothermal cancer cell killing efficacy. This work presents a facile approach to synthesize water-soluble noble metal coated SWNTs with a strong SERS effect suitable for labeling and fast Raman spectroscopic imaging of biological samples, which has been rarely realized before. The SWNT-Au-PEG nanocomposite developed here may thus be an interesting optical theranostic probe for cancer imaging and therapy.



INTRODUCTION

Carbon nanotubes, especially single-walled carbon nanotubes (SWNTs), have attracted significant interest in the area of biomedicine, for potential applications in biological detection, drug delivery, phototherapies, and biomedical imaging.^{1–7} Owing to their unique one-dimensional (1-D) structure, SWNTs exhibit strong resonance Raman scattering due to their sharp electronic density of states at the van Hove singularities.¹ SWNTs have several distinctive Raman scattering features, including the radial breathing mode (RBM) and tangential mode (G-band),⁸ which are sharp and strong peaks that can be easily distinguished from fluorescence backgrounds and are thus suitable for optical Raman imaging. Raman imaging of SWNTs in live cells was first reported by Heller et al. in 2005.⁹ Targeted *in vivo* Raman imaging was already realized by Zavaleta et al.¹⁰ in 2008. SWNTs with different isotope compositions showed shifted G-band peaks¹¹ and could be used as different “colors” for Raman imaging under a single laser excitation.^{7,12} Compared with fluorescence dyes, Raman scattering of SWNTs is resistant to quenching and photo-bleaching,¹ suitable for long-term tracking and labeling.^{13,14}

However, although SWNTs likely exhibit the strongest inherent Raman scattering among all “single molecules” (one nanotube can be deemed as a single conjugated molecule), a relatively long spectral acquisition time (0.5–1 s) is usually needed at each pixel during Raman spectroscopic imaging, resulting in a rather long imaging time to obtain one Raman image (a few hours for a 100 × 100 image).

Surface enhanced Raman scattering (SERS) is able to enhance Raman signals of molecules adsorbed on rough noble metal surfaces or nanoparticles by as high as many orders of magnitude, and it has been widely investigated in the past few decades for applications in single molecule detection and in chemical and biological sensing, as well as biomedical imaging.^{15–18} SERS studies with SWNTs have also gained particular interest.^{19–23} Chen and co-workers made a network of silver nanoparticle-deposited SWNTs, which showed a strong correlation between localized surface plasmon resonance wavelength, particle size and density, laser excitation wave-

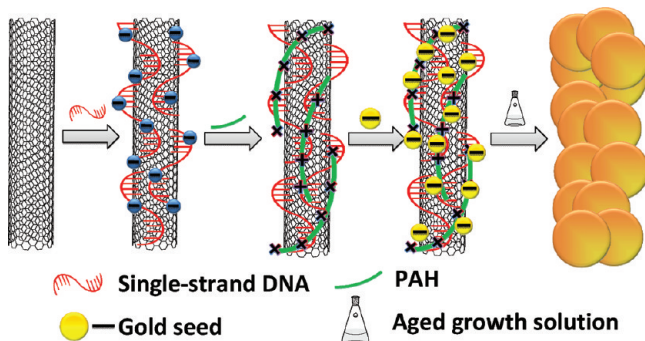
Received: January 5, 2012

Published: April 9, 2012

length, and degree of Raman enhancement.¹⁹ To detect every nanotube on surface-grown SWNTs, Li and co-workers developed an chemical deposition method comprised of seed formation and subsequent seeded growth to deposit gold nanoparticles on the surface of SWNTs.²⁰ The average SERS enhancement factors of G-band intensity after gold decoration were 6.4, 54, and 97 upon excitation with laser wavelengths of 442, 633, and 785 nm, respectively. Utilizing on-substrate SERS of SWNTs (~60 times of SERS enhancement), ultrasensitive sensing of biological molecules was achieved by Dai and co-workers.²¹ Besides depositing noble metal nanoparticles on substrate and solid samples of SWNTs for SERS studies, soluble-phase SERS of SWNTs has also been reported by attaching/growing gold nanoparticles on covalently functionalized SWNTs (e.g., oxidized SWNTs).^{22,23} However, covalent functionalization could largely destroy the nanotube structure and drastically decrease Raman signals of SWNTs by many orders of magnitude. To develop SWNT-based nanoprobes with ultrastrong Raman signals for fast Raman imaging of biological samples, pristine SWNTs with noncovalent functionalization have to be used to fabricate water-soluble SERS nanocomposites in the solution phase, which unfortunately have not yet been achieved to our best knowledge.

Here, we report an *in situ* solution phase synthesis method to grow noble metal nanoparticles onto noncovalently functionalized SWNTs (Scheme 1). Single-strand DNA (ssDNA) is

Scheme 1. Schematic Illustration of the Synthetic Procedure of SWNTs-Metal Nanocomposite



employed to functionalize pristine SWNTs, offering negatively charged DNA coated nanotubes, onto which positively charged poly(allylamine hydrochloride) (PAH) is adsorbed by electrostatic force. After attaching negatively charged gold seeds to the surface of DNA/PAH coated SWNTs (SWNT-DNA-PAH), a seeded nanocrystal growth is carried out to obtain SWNT-Au and SWNT-Ag nanocomposites, which are further stabilized by the biocompatible PEG coating. The noble metal coated SWNTs gain excellent SERS effects, with the maximal enhancement factor of over 20. After conjugating the SWNT-Au-PEG nanocomposite with a targeting ligand, folic acid (FA), selective cancer cell labeling and fast Raman imaging are realized using SWNT-Au-PEG-FA, which can also serve as an excellent photothermal agent for cancer cell ablation.

RESULTS AND DISCUSSION

SWNT-metal nanocomposites were synthesized in the solution phase using *in situ* gold seed attachment and seeded growth methods through a layer-by-layer (LBL) self-assembly procedure. Raw SWNTs were first modified by ssDNA through

noncovalent binding to acquire water solubility. A cationic polymer, PAH, was then used to coat DNA functionalized SWNTs (SWNT-DNA) by electrostatic interaction, offering SWNTs positive charges. No obvious aggregation of nanotubes was noticed during this step after PAH binding (Supporting Information Figure S1). The ζ potential increased from -23 mV for SWNT-DNA to $+24$ mV for SWNT-DNA-PAH (Supporting Information Figure S2), indicating the successful PAH binding on SWNT-DNA. Negatively charged gold seeds grown in aqueous NaOH were then added in large excess and attached to the surface of SWNT-DNA-PAH. After removal of unattached gold seeds, the ζ potential of nanotubes was measured to be -15.1 mV, a remarkable decrease from that of SWNT-DNA-PAH as the result of gold seeds attachment.

Small gold seeds attached on the surface of SWNTs then acted as nucleation sites to induce seeded gold/silver growth, after which both SWNT-Au and SWNT-Ag nanocomposites with fine structures were synthesized. Lipoic acid modified PEG (LA-PEG) was then introduced to stabilize the nanocomposites, obtaining SWNT-Au-PEG and SWNT-Ag-PEG stable in various physiological solutions including serum (Supporting Information Figure S3). SEM and TEM images (Figure 1a–c) of the synthesized SWNT-Au-PEG nanocomposite at the optimized condition (added with 4 mM of gold growth solution) revealed that gold nanoparticles with relatively uniform sizes of about 40–50 nm were densely decorated on the SWNT–surface after seeded growth, while adding lower or higher concentrations of gold growth solutions resulted in much different structures (Supporting Information Figure S4). Compared to SWNT-Au-PEG, silver nanoparticles in the SWNT-Ag-PEG sample were obviously bigger in size, with diameters of 70–150 nm (Figure 1d–f). The elemental composition determined by energy-dispersive X-ray spectroscopy (EDS) further evidenced the composition of SWNT-metal composites (Figure 1g). UV-vis/NIR spectra of SWNT-DNA and SWNT-metal composites (Figure 1h) displayed the absorption peaks around 440 nm for SWNT-Ag-PEG and about 580 nm for SWNT-Au-PEG, both of which showed a dramatic increase compared to DNA functionalized SWNTs. It is worth noting that after the growth of gold shells surrounding cylinder SWNTs, a continuous absorption band from the visible to NIR regions appeared for SWNT-Au-PEG (Figure 1h, the red line). The strong surface plasmon resonance NIR absorption contributed by the gold shell on SWNTs could be utilized to enhance Raman scattering of nanotubes by SERS under NIR excitation, and it also could be useful for enhanced photothermal ablation of cancer cells.^{24–26}

We next carefully studied the SERS enhancement factors (EFs) of SWNT-Au-PEG and SWNT-Ag-PEG samples prepared under varied conditions. The digital photos of SWNT-Au-PEG and SWNT-Ag-PEG solutions synthesized by introducing different concentrations of aged Au/Ag growth solutions (Figure 2a and b) clearly showed the color change as addition of growth solutions. Raman spectra of various SWNT-Au-PEG and SWNT-Ag-PEG nanocomposites at the same nanotube concentration were recorded under two different laser excitations (633 and 785 nm) (Figure 2c–h). As for SWNT-Au-PEG, under both 633 nm and 785 nm laser excitations, the SERS EFs first rose as the increase of added growth solution concentrations and reached the optimum condition at ~4 mM, after which an obvious decrease of EF values was observed by further increasing the concentration of gold growth solution (Figure 2c–e), likely owing to the

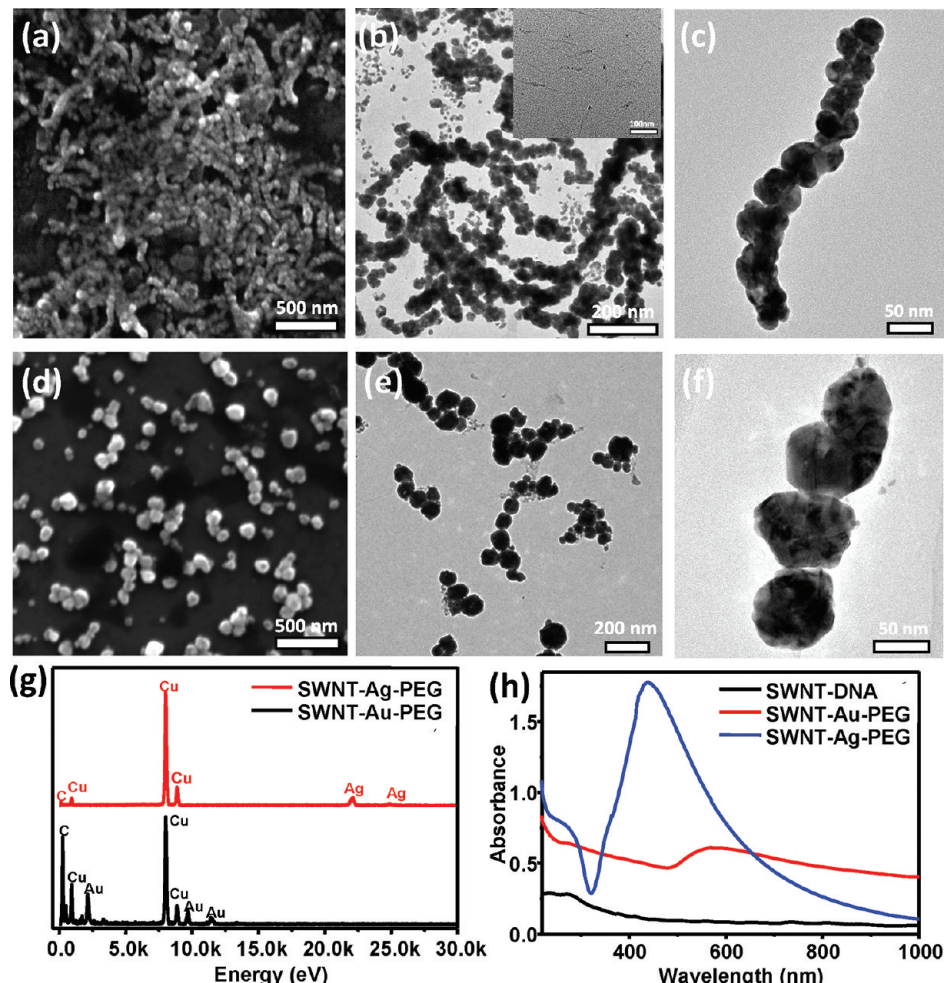


Figure 1. Characterization of SWNT-Au-PEG and SWNT-Ag-PEG nanocomposites. (a–c) Representative SEM (a) and TEM (b and c) images of the SWNT-Au-PEG nanocomposite. The inset in (b) is a TEM image of DNA modified SWNTs. (d–f) Representative SEM (d) and TEM (e and f) images of the SWNT-Ag-PEG nanocomposite. (g) EDS of the SWNT-Au-PEG (red line) and SWNT-Ag-PEG (black line) nanocomposites under the STEM pattern. (h) UV-vis/NIR absorption spectra of SWNT-DNA (10 nM), SWNT-Au-PEG, and SWNT-Ag-PEG solutions (1 nM by SWNT content). The above characterization data were obtained using selected SWNT-Au-PEG and SWNT-Ag-PEG samples with the optimum SERS effect (Figure 2).

formation of irregular aggregates with large sizes (Supporting Information Figure S4). The maximal SERS EFs at the optimum condition (4 mM gold aged growth solution) were ~7.7 and ~12.6, under 633 and 785 nm excitation, respectively. The SERS enhancement of SWNT-Ag-PEG under 633-nm excitation followed the same trend as that of SWNT-Au-PEG, with the maximal EF of 26.5 at 5 mM of silver growth solution (Figure 2f and h). However, when excited with the 785 nm laser, the EFs of SWNT-Ag-PEG were much lower, showing a maximal EF of ~8.7 (Figure 2g and h), likely due to the relatively weak plasmonic absorption of Ag nanostructures at longer wavelength. At the optimized preparation conditions for SWNT-Au-PEG and SWNT-Ag-PEG, 10 nM of SWNTs was coated with 0.38 mg/mL of Au and 2.69 mg/mL of Ag, respectively, as determined by inductively coupled plasma-atomic emission spectrometry (ICP-AES) measurement.

Under 785 nm excitation, both exciting and scattering photons are in the NIR window (700–900 nm) with the lowest tissue absorption and autofluorescence background, ideal for optical imaging in biological systems.^{1,12} SWNT-Au-PEG exhibits stronger NIR plasmonic absorption and higher SERS EF under 785 nm excitation than SWNT-Ag-PEG. Moreover,

compared to silver, gold is more inert in its chemical property and may show relatively better biocompatibility.^{24,27–29} We thus chose SWNT-Au-PEG for our followed biomedical studies.

A standard cell toxicity test was carried out first to determine the cytotoxicity of the as synthesized SWNT-Au-PEG before it was used for further biological experiments. The experimental results revealed no obvious toxic effect of our SWNT-Au-PEG on treated cells at tested concentrations (Supporting Information Figure S5).

To achieve selective labeling of a specific type of cancer cells, folic acid conjugated LA-PEG (LA-PEG-FA) was used to stabilize as-made SWNT-Au, obtaining SWNT-Au-PEG-FA to target the folate receptor (FR), which is widely known to be up-regulated in many types of cancer cells. FR-positive human epidermoid carcinoma KB cells cultured in an FA-free medium and FR-negative HeLa cells cultured in a normal medium were incubated with SWNT-Au-PEG or SWNT-Au-PEG-FA (5 nM) for 30 min and washed extensively with phosphate buffered saline (PBS) before Raman imaging (Figure 3a–d). SWNT-PEG and SWNT-PEG-FA (5 nM) were used as the control to

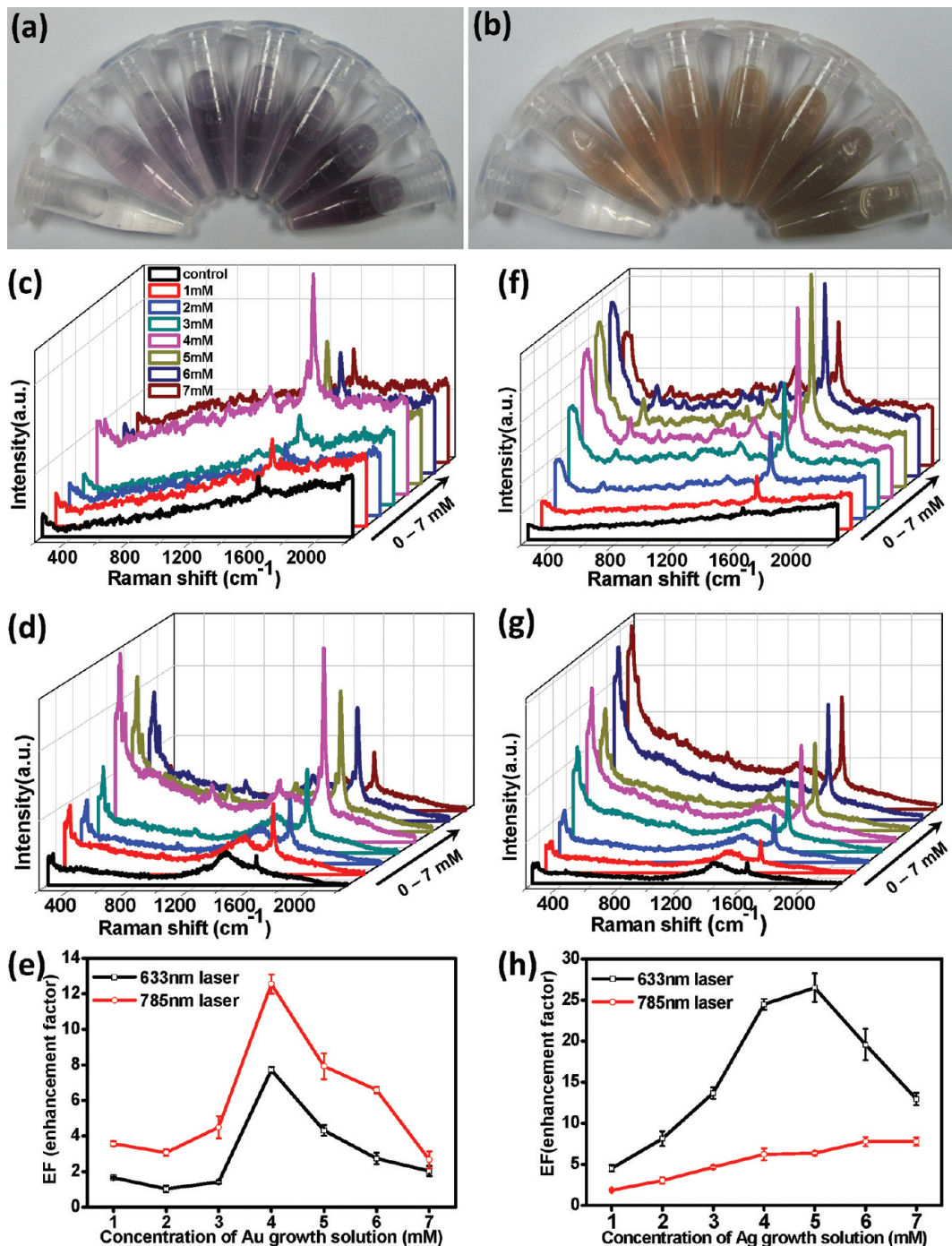


Figure 2. Studies on the SERS effects. (a and b) Photos of SWNT-Au-PEG (a) and SWNT-Ag-PEG (b) solutions prepared by adding different concentrations of aged growth solutions. From left to right were samples added with increasing concentrations of growth solutions (0 mM to 7 mM). All the samples were diluted 5 times by DI water before photos were taken. (c and d) Raman spectra of SWNT-Au-PEG prepared by adding different concentrations of growth solutions taken under 633 nm (c) and 785 nm (d) laser excitation. (f and g) Raman spectra of SWNT-Ag-PEG samples prepared by adding different concentrations of silver growth solutions taken under 633 nm (f) and 785 nm (g) laser excitation. (e and h) SERS EFs of SWNT-Au-PEG (e) and SWNT-Ag-PEG (h) samples with increasing concentrations of growth solutions. Error bars were based on three parallel measurements for each sample.

reveal the benefit of SERS for SWNT-based cell labeling and Raman imaging (Figure 3e–h).

Raman imaging of cells was conducted by a Horiba-JY confocal Raman microscope using a 785 nm laser as the excitation source. To ensure fast Raman scanning, a rather short integration time (0.1 s per pixel) was used in combination with the SWIFT ultrafast Raman mapping model. Under our

imaging condition, strong Raman signals were observed for KB cells incubated with SWNT-Au-PEG-FA, while cells incubated with SWNT-Au-PEG showed much weaker signals, suggesting selective binding of SWNT-Au-PEG-FA on FR positive cancer cells, which was also evidenced by TEM images of cell samples (Supporting Information Figure S6). As expected, no obvious Raman signals were noted from HeLa

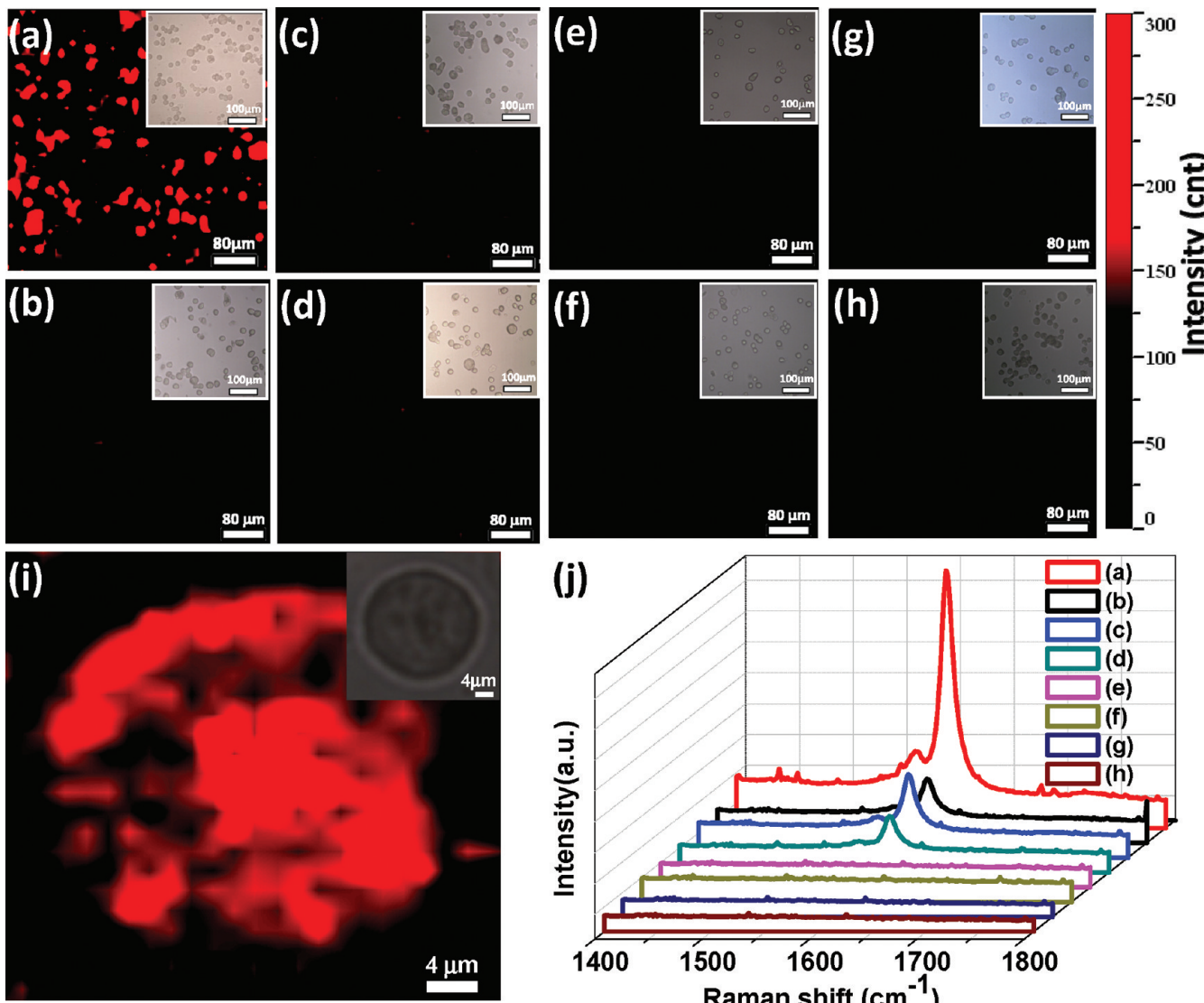


Figure 3. Raman imaging of cells. (a–h) Raman images of SWNT-Au-PEG-FA (a and b), SWNT-Au-PEG (c and d), SWNT-PEG-FA (e and f), and SWNT-PEG (g and h) labeled KB (a, c, e, g) and HeLa (b, d, f, h) cells. The nanotube concentrations in all samples were kept constant at 5 nM. (i) High-resolution Raman image of a SWNTs-Au-PEG-FA labeled KB cell. The insets in parts a–i corresponded to bright field images of cells. (j) Averaged Raman spectra in each image from (a) to (h). The step size was 8 μm in images (a–h) and 1.5 μm in (i). The intensity of the SWNT Raman G-band peak at 1590 cm^{-1} was used to contrast the above Raman spectroscopic images.

cells after incubation with either SWNTs-Au-PEG or SWNTs-Au-PEG-FA. In marked contrast, KB cells labeled with SWNT-PEG-FA showed neglectable Raman signals at our experimental conditions (0.1 s integration time per pixel), due to the relatively low Raman intensity of nanotubes without SERS. As semiquantification, all Raman spectra in each Raman spectroscopic image were integrated (Figure 3j), showing excellent labeling specificity of SWNT-Au-PEG-FA and dramatically increased Raman labeling performance of Au coated SWNTs as compared to plain SWNTs without SERS.

The key benefit of using Au decorated SWNTs as Raman probes for cell imaging is the short imaging time owing to the strongly enhanced Raman signals by SERS. The time taken to acquire one Raman image could be as short as a few minutes in this work, a remarkable decrease from the few hours needed in previous SWNT-based Raman imaging of cells (1–2 s integration time at each pixel). In another control experiment, we compared Raman images of SWNT-Au-PEG-FA labeled KB

cells and SWNT-PEG-FA labeled cells (Supporting Information Figure S7). While a 0.1 s integration time (~6 min for one 50 × 50 image) was enough to obtain sufficient Raman signals using SWNT-Au-PEG-FA as the Raman probe, a long integration time of 1 s at each pixel (~1 h for one 50 × 50 image) is necessary to collect sufficient signals for a decent Raman spectroscopic image of cells labeled with unmodified SWNT-PEG-FA (Supporting Information Figure S7). The absolute signals in the latter image were still slightly weaker than the former, despite the 10× imaging time used.

Both carbon nanotubes and gold nanomaterials with strong light absorbing capabilities have been widely explored in the photothermal therapy (PTT) of cancer.^{3,25,26,30,31} The growth of the gold shell dramatically increased the optical absorbance of the SWNT-based nanocomposite in the NIR region. We thus explored the enhanced photothermal ablation of cancer cells with our SWNT-Au-PEG nanocomposites. When exposed to an 808 nm NIR laser at a power density of 1W/cm², the

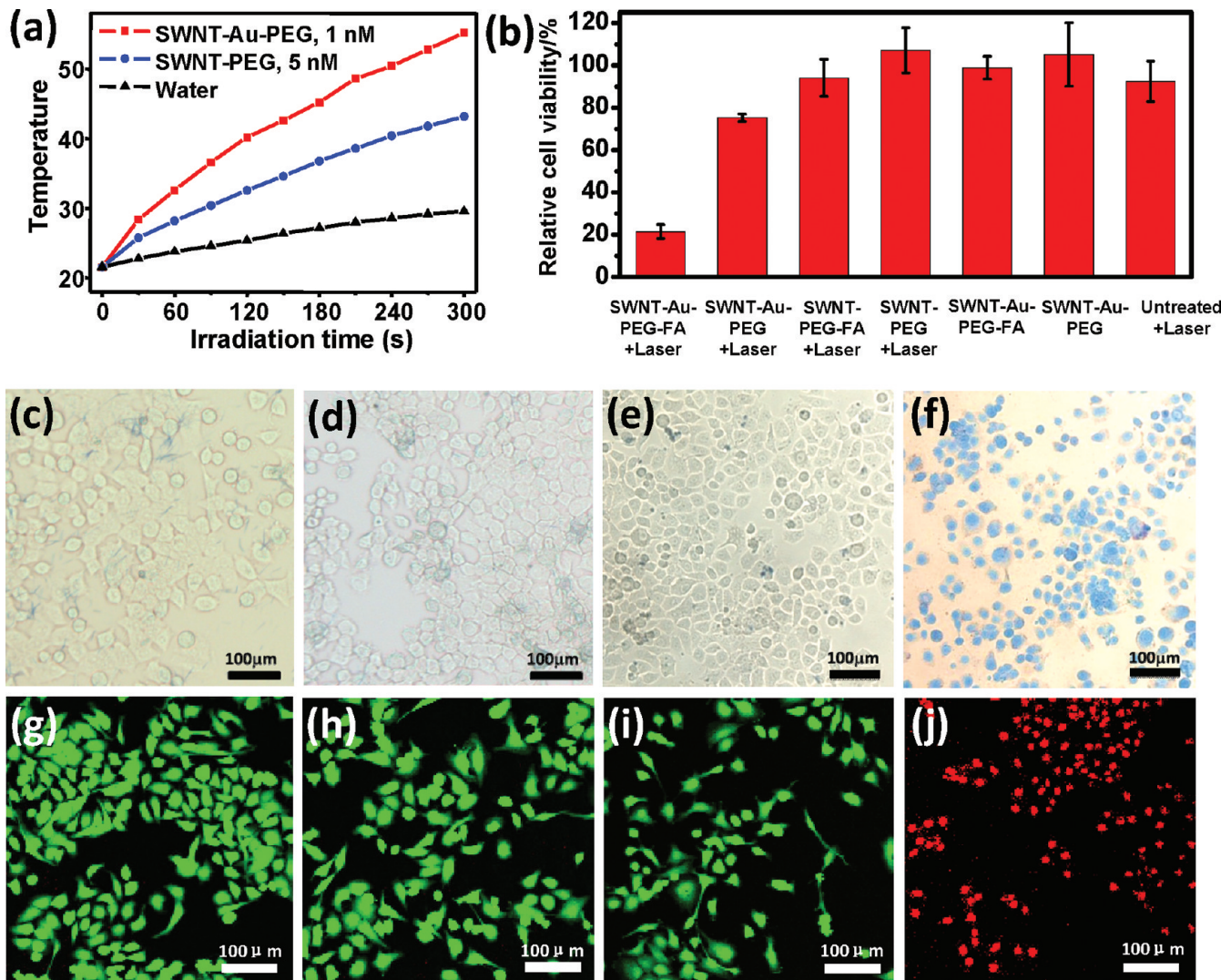


Figure 4. Targeted photothermal ablation of cancer cells. (a) The heating curves of water and the SWNT-PEG (5 nM by SWNT) and SWNT-Au-PEG nanocomposites (1 nM by SWNT) under 808 nm laser irradiation at a power density of 1 W/cm². (b) Relative cell viabilities of SWNT-Au-PEG-FA, SWNT-Au-PEG, SWNT-PEG-FA, and SWNT-PEG treated KB cells with or without laser irradiation (808 nm, 1 W/cm², 5 min). (c–f) Optical microscopy images of trypan blue stained KB cells after being incubated with SWNT-PEG (c), SWNT-PEG-FA (d), SWNT-Au-PEG (e), or SWNT-Au-PEG-FA (f), and then exposed to the laser irradiation. The nanotube concentration was 5 nM in all above samples. (g–j) Confocal fluorescence images of calcein AM (green, live cells)/propidium iodide (red, dead cells) costained KB cells bearing the same PTT treatment as that in parts c–f.

SWNT-Au-PEG solution (1 nM by SWNT content) showed a nearly 30 °C of temperature rise within 5 min. In contrast, the temperature change of the SWNT-PEG solution (5 nM) was much less significant under the same laser irradiation conditions.

For targeted cancer cell ablation, KB cells were incubated with SWNT-Au-PEG-FA, SWNT-Au-PEG, SWNT-PEG-FA, and SWNT-PEG, respectively, at the same nanotube concentration. After laser irradiation of 808 nm for 5 min at the power density of 1 W/cm², relatively cell viabilities were determined (Figure 4b). The majority of KB cells treated with SWNT-Au-PEG-FA were killed after laser irradiation, while SWNT-Au-PEG treated cells showed much less cell death after exposure to the NIR laser. In contrast, either SWNT-PEG-FA or SWNT-PEG treated cells showed negligible cell death after laser irradiation. Bright field microscopy images of trypan blue stained cells and confocal fluorescence microscopy images of Calcein AM/Propidium iodide (PI) costained cells after various treatments (Figure 4c–j) provided the same information.

These results clearly demonstrate that the SWNT-Au nanocomposite has much better photothermal therapeutic effect than plain SWNTs. Control experiments on FR negative HeLa cells uncovered no appreciable cell death after SWNT-Au-PEG-FA incubation and laser irradiation, further evidencing that the photothermal ablation of cancer cells was highly selective (Supporting Information Figure S8).

To demonstrate the advantage of our SWNT-Au nanocomposite over gold nanostructures used in PTT, we compared its photostability with gold nanorods (AuNRs, length = 41–45 nm, width = 11–13 nm). After 808-nm laser irradiation for 60 min at 1 W/cm², PEGylated AuNRs (AuNR-PEG) solution lost the majority of its absorbance at 808 nm, while the SWNT-Au-PEG solution merely decreased to 87% of its initial absorbance (Figure 5a–c). The color of AuNR-PEG changed from dark pink to nearly colorless, while the color of SWNT-Au-PEG showed no apparent change (Figure 5d). The decrease in the absorbance of AuNRs under laser irradiation is a problem in AuNR-based PTT applications, and owing to the morphology

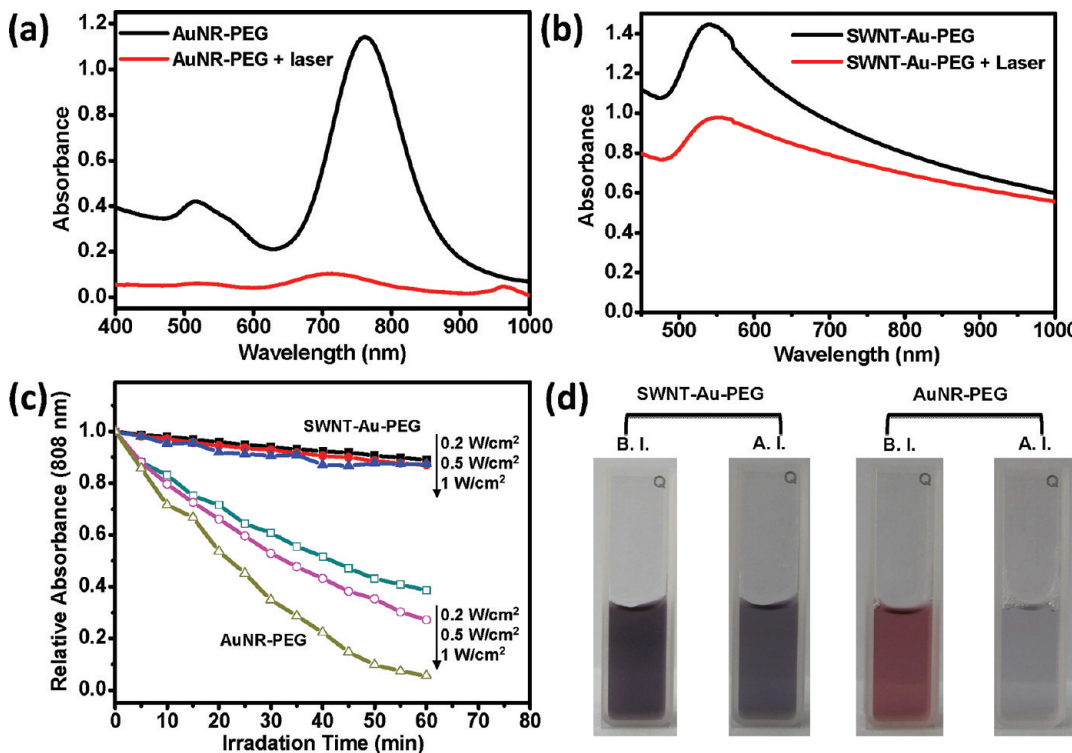


Figure 5. Comparison of photostability between SWNT-Au-PEG and AuNR-PEG under 808-nm laser irradiation. (a and b) UV/vis/NIR absorption spectra of AuNR-PEG (a) and SWNT-Au-PEG (b) solutions before and after laser irradiation (1 W/cm^2 for 1 h). (c) Change of relative absorbance at 808 nm for SWNT-Au-PEG and AuNR-PEG solutions under laser exposure at different power densities ($0.2\text{--}1 \text{ W/cm}^2$). (d) Photos of SWNT-Au-PEG and AuNR-PEG solutions before irradiation (B.I.) and after the laser irradiation (A.I.) at 1 W/cm^2 for 1 h.

change (melting) of nanorods under local heating (Supporting Information Figure S9).^{32,33} With a nanotube as the backbone, the SWNT-Au nanostructure, which also looks like a “nanorod”, may be more resistant to melting under photo-induced local heating.

CONCLUSIONS

In summary, an *in situ* synthetic method has been developed to decorate noble metal nanoparticles onto noncovalently functionalized SWNTs with high density in the solution phase, obtaining SWNT-Au-PEG and SWNT-Ag-PEG nanocomposites which exhibit excellent concentration and excitation-source dependent SERS effects. Utilizing FA conjugated SWNT-Au-PEG-FA, selective cancer cell labeling and Raman imaging is realized, with remarkably shortened imaging time compared to that of using a nonenhanced SWNT-nanoprobe, owing to the strongly enhanced Raman signals of nanotubes by SERS. Moreover, the SWNT-Au-PEG-FA nanocomposite also exhibits dramatically improved photothermal cancer cell killing efficacy due to the strong surface plasmon resonance absorption contributed by the gold shell grown on the nanotube surface. The photothermal stability of SWNT-Au-PEG is found to be significantly higher than that of AuNR-PEG. Combining the intrinsic properties of both SWNTs and gold, the SWNT-Au nanocomposite developed here may be an interesting nanoplatform promising in biosensing, optical imaging, and phototherapy.

EXPERIMENTAL SECTION

Seed-Mediated Ag/Au Growth on SWNTs. Noncovalent Coating of Charged Polymers on SWNTs. Noncovalent functionalization of SWNTs with DNA has been well established in

earlier reports.^{34–37} A DNA solution with the sequence of 5'-ATTCGCGACTCGCGA-3' (Sangon Biotech) at a concentration of $20 \mu\text{M}$ was sonicated with raw Hipco SWNTs (0.15 mg/mL) for 1 h. The SWNT-DNA suspension was then centrifuged at 14000 rpm for 1 h to remove aggregates. Excess DNA in the supernatant was then removed by filtration through 100 kDa ultracentrifugal filter devices (Millipore Amicon Ultra). DNA coated SWNTs with negative charges were then modified by poly(allylamine hydrochloride) (PAH, purchased from Sigma Inc.). One milliliter of PAH (10 mg/mL) was added to 5 mL of 200 nM SWNT-DNA (calculated by the extinction coefficient at 808 nm: $\epsilon_{808 \text{ nm}} = 7.9 \times 10^6 \text{ M}^{-1} \text{ cm}^{-1}$)³⁸ under rigorous stirring. After continued stirring overnight, the mixture was briefly sonicated for a few seconds to obtain a homogeneous solution, which was then thoroughly washed with deionized (DI) water by filtration through 100-nm filter membrane (Millipore) to remove excess PAH.

Attachment of Gold Seeds on SWNTs. Negatively charged gold seeds were synthesized following a reported protocol³⁹ by reduction of hydrogen tetrachloroaurate (III) hydrate (HAuCl_4) with tetrakis(hydroxymethyl)phosphonium chloride (THPC) in a solution of NaOH. SWNT-DNA-PAH was attached with gold seeds by mixing 2 mL of 200 nM SWNT-DNA-PAH with 20 mL of gold seeds solution. After stirring at room temperature for 4 h, excess unattached gold seeds were removed by centrifugation at 14800 rpm with supernatants discard, and washed with DI water for 2–3 times.

Preparation of Growth Solutions. An aged gold growth solution was prepared by mixing 2 mL of 25 mg/mL potassium carbonate (K_2CO_3) with 4 mL of 1 wt % HAuCl_4 in 200 mL of DI water. The color of the mixture changed from yellow to colorless within 30 min. Silver growth solution was prepared using an analogous procedure (added 2 mL of 1 wt % AgNO_3 instead of $\text{HAuCl}_4 \cdot \text{H}_2\text{O}$). The solution was aged for 1 day before use.⁴⁰

Seed Mediated Au/Ag Growth on SWNTs. SWNT-Au and SWNT-Ag nanocomposites were then synthesized by a seeded growth

procedure, with small gold seeds attached on the surface of SWNTs as nucleation centers. To grow gold nanoparticles onto SWNTs, 200 μL of gold seeds attached SWNTs (50 nM) was added with varying amounts of aged gold growth solution (1.7–11.9 mL). After stirring the mixture for 10 min, various volumes of formaldehyde (37%, 8.5–59.5 μL) were added as the reducing agent. The solution color changed from colorless to pink and then purple during the reaction. SWNT-Ag nanocomposite was prepared in the same manner, but with a mixture of formaldehyde and ammonium hydroxide (25–175 μL) as the reducing agent. For the control samples, DI water was added instead of aged Au/Ag growth solutions.

PEGylation of SWNT–Metal Nanocomposites. Lipoic acid modified PEG (LA-PEG) and folic acid conjugated LA-PEG (LA-PEG-FA) were synthesized following a reported protocol⁴¹ and used to stabilize as-made SWNT-Ag and SWNT-Au nanocomposites. To 1 mL of SWNT-Ag or SWNT-Au solution, 5 mg of LA-PEG or LA-PEG-FA was added at ~20 min after the Ag/Au nanoparticle growth was initiated (by adding reducing agents). Excess reagents were removed by centrifugation at 14800 rpm and repeated water washing. For biological experiments, SWNT-Au-PEG and SWNT-Au-PEG-FA were further dialyzed against DI water using 3500 Da MWCO membranes to remove residual ions.

Synthesis of SWNT-PEG and SWNT-PEG-FA. PEG-grafted poly(maleic anhydride-*alt*-1-octadecene) (PMHC₁₈-mPEG) and the one with folic acid modification (PMHC₁₈-mPEG-FA) was synthesized following our previously reported protocols.^{3,42,43} SWNT-PEG and SWNT-PEG-FA were synthesized by sonicating raw SWNTs (0.2 mg/mL) in aqueous solutions of PMHC₁₈-mPEG or PMHC₁₈-mPEG-FA (3 mg/mL), respectively, for 1 h. The PEGylated SWNT suspensions were then centrifuged at 14000 rpm for 1 h to remove aggregates. The supernatants were thoroughly washed with DI water by filtration through a 100 nm filter membrane (Millipore) to remove excess polymers.

Synthesis of AuNR-PEG. AuNRs were synthesized following a well established protocol in a solution of cetyl-trimethylammonium bromide (CTAB).⁴⁴ After removal of excess CTAB from as-made AuNRs by centrifugation and water washing, LA-PEG (5 mg/mL) was added to stabilize AuNRs. After stirring for 4–6 h, the remaining CTAB, which fell down from Au nanorods by ligand exchange as well as excess LA-PEG, was also removed by centrifugation.

Characterizations. Scanning electron microscopy (SEM) images were taken by using a FEI Quanta 200F scanning electron microscope. Transmission electron microscopy (TEM) images were obtained using a Philips CM300 transmission electron microscope operating at an acceleration voltage of 200 kV. All TEM samples were deposited on 300 mesh holey carbon-coated copper grids and dried overnight before examination. UV/vis spectra were obtained with a PerkinElmer Lambda 750 UV/vis spectrophotometer over the wavelength range 200–1000 nm. Raman spectra were taken using a Raman spectrometer (Horiba LabRam HR 800) for SWNT samples in the solution phase loaded in capillary tubes, with the laser beam focused on the center of a tube in both the longitude and transverse directions.

Raman Imaging of Cells. All cell culture-related agents were purchased from Invitrogen. Human carcinoma KB cells and HeLa cells obtained from the American Type Culture Collection (ATCC) were cultured in folate acid free RPMI-1640 and completed high-glucose DMEM cell medium, respectively, both supplemented with 10% fetal bovine serum (FBS) and 1% penicillin/streptomycin. For Raman imaging, 200 μL of KB or HeLa cells were incubated with SWNT-PEG, SWNT-PEG-FA, SWNT-Au-PEG, and SWNT-Au-PEG-FA solutions for 0.5 h at 4 °C. The final concentrations in these incubation solutions were all 5 nM in term of nanotube concentration. After washing with phosphate buffered saline (PBS) for three times, cells were fixed by 2.5% glutaraldehyde and imaged under a Raman confocal microscope (Horiba LabRam HR 800) with a 785 nm laser (80 mW) as the excitation light source. A drop of cell suspension (about 10–20 μL) was sealed between two thin quartz cover-slides for imaging. A 50× objective lens (~1 μm laser spot size) was used, and the pinhole was selected as 400 μm . Each Raman spectroscopic map (Figure 3a–i) contains at least 50 × 50 spectra, with 0.1 s integration time for each

spectrum. Step sizes of 8 μm and 1.5 μm were used for Raman mapping to obtain large area images (Figure 3a–h) and high resolution images (Figure 3i), respectively.

Selective Photothermal Ablation of Cancer Cells. For photothermal therapy, KB cells were precultured in 96-well cell culture plates at 1 × 10⁴/well for 24 h and then added with SWNT-PEG, SWNT-PEG-FA, SWNT-Au-PEG, or SWNT-Au-PEG-FA at the tested concentration (5 nM). After incubation for 0.5 h at 4 °C, cells were washed with PBS to remove excess nanomaterials and then incubated at 37 °C for another 2 h to allow the internalization of nanotubes. An 808 nm NIR laser was used to irradiate cells at a power density of 1 W/cm² for 5 min. The standard cell viability assay using 3-(4,5-dimethylthiazol-2-yl)-2,5-diphenyltetrazolium bromide (MTT, Sigma Inc.) was carried out to determine the cell viabilities relative to the control cells incubated with the same volume of PBS. For trypan blue staining, KB cells (2 × 10⁵ cells) grown in the FBS containing medium cultured in 35 mm culture dishes were irradiated by the 808 nm laser after incubation with SWNT-PEG, SWNT-PEG-FA, SWNT-Au-PEG, or SWNT-Au-PEG-FA, washed with PBS, and stained with 0.04% Trypan blue solution (Sigma Inc.) for 5 min. Microscopic images of cells were then taken using a Leica microscope.

ASSOCIATED CONTENT

Supporting Information

Zeta potential measurement during the synthesis procedure, characterization of SWNT-DNA-PAH, photos of SWNT-Au-PEG and SWNT-Ag-PEG in various physiological solutions, in vitro cellular toxicity assay of SWNT-Au-PEG, TEM images of cell samples, Raman imaging of KB cells incubated with SWNT-Au-PEG-FA and SWNT-PEG-FA, and TEM images of AuNR-PEG before and after laser irradiation. This material is available free of charge via the Internet at <http://pubs.acs.org>.

AUTHOR INFORMATION

Corresponding Author

zliu@suda.edu.cn

Notes

The authors declare no competing financial interest.

ACKNOWLEDGMENTS

(This work was supported by the National Basic Research Program (973 Program) of China (2012CB932601, 2011CB911002), the National Natural Science Foundation of China (51072126, 51002100, 51132006), the Research Grants Council of Hong Kong SAR-CRF Grant (CityU5/CRF/08), and a Project Funded by the Priority Academic Program Development of Jiangsu Higher Education Institutions.

REFERENCES

- Liu, Z.; Tabakman, S.; Welsher, K.; Dai, H. *Nano Res.* **2009**, *2*, 85.
- Liu, Z.; Yang, K.; Lee, S.-T. *J. Mater. Chem.* **2011**, *21*, 586.
- Liu, X.; Tao, H.; Yang, K.; Zhang, S.; Lee, S.-T.; Liu, Z. *Biomaterials* **2011**, *32*, 144.
- Yang, W.; Ratinac, K. R.; Ringer, S. P.; Thordarson, P.; Gooding, J. J.; Braet, F. *Angew. Chem., Int. Ed.* **2010**, *49*, 2114.
- Kam, N. W. S.; Dai, H. *J. Am. Chem. Soc.* **2005**, *127*, 6021.
- Kam, N.; Liu, Z.; Dai, H. *J. Am. Chem. Soc.* **2005**, *127*, 12492.
- Liu, Z.; Li, X.; Tabakman, S.; Jiang, K.; Fan, S.; Dai, H. *J. Am. Chem. Soc.* **2008**, *130*, 13540.
- Rao, A. M.; Richter, E.; Bandow, S.; Chase, B.; Eklund, P. C.; Williams, K. A.; Fang, S.; Subbaswamy, K. R.; Menon, M.; Thess, A.; Smalley, R. E.; Dresselhaus, G.; Dresselhaus, M. S. *Science* **1997**, *275*, 187.
- Heller, D. A.; Baik, S.; Eurell, T. E.; Strano, M. S. *Adv. Mater.* **2005**, *17*, 2793.

- (10) Zavaleta, C.; De La Zerda, A.; Liu, Z.; Keren, S.; Cheng, Z.; Schipper, M.; Chen, X.; Dai, H.; Gambhir, S. *Nano Lett.* **2008**, *8*, 2800.
- (11) Liu, L.; Fan, S. *J. Am. Chem. Soc.* **2001**, *123*, 11502.
- (12) Liu, Z.; Tabakman, S.; Sherlock, S.; Li, X.; Chen, Z.; Jiang, K.; Fan, S.; Dai, H. *Nano Res.* **2010**, *3*, 222.
- (13) Wang, C.; Ma, X.; Ye, S.; Cheng, L.; Yang, K.; Guo, L.; Li, C.; Li, Y.; Liu, Z. *Adv. Funct. Mater.* **2012**, DOI: 10.1002/adfm.201200133.
- (14) Liu, Z.; Davis, C.; Cai, W.; He, L.; Chen, X.; Dai, H. P. *Natl. Acad. Sci. U.S.A.* **2008**, *105*, 1410.
- (15) Nie, S.; Emory, S. R. *Science* **1997**, *275*, 1102.
- (16) Qian, X.; Peng, X.-H.; Ansari, D. O.; Yin-Goen, Q.; Chen, G. Z.; Shin, D. M.; Yang, L.; Young, A. N.; Wang, M. D.; Nie, S. *Nat. Biotechnol.* **2008**, *26*, 83.
- (17) Cao, Y. C.; Jin, R.; Mirkin, C. A. *Science* **2002**, *297*, 1536.
- (18) Zavaleta, C. L.; Smith, B. R.; Walton, I.; Doering, W.; Davis, G.; Shojaei, B.; Natan, M. J.; Gambhir, S. S. *Proc. Natl. Acad. Sci. U.S.A.* **2009**, *106*, 13511.
- (19) Chen, Y.-C.; Young, R. J.; Macpherson, J. V.; Wilson, N. R. *J. Phys. Chem. C* **2007**, *111*, 16167.
- (20) Chu, H.; Wang, J.; Ding, L.; Yuan, D.; Zhang, Y.; Liu, J.; Li, Y. *J. Am. Chem. Soc.* **2009**, *131*, 14310.
- (21) Chen, Z.; Tabakman, S. M.; Goodwin, A. P.; Kattah, M. G.; Daranciang, D.; Wang, X.; Zhang, G.; Li, X.; Liu, Z.; Utz, P.; Jiang, K.; Fan, S.; Dai, H. *Nat. Biotechnol.* **2008**, *26*, 1285.
- (22) Beqa, L.; Singh, A. K.; Fan, Z.; Senapati, D.; Ray, P. C. *Chem. Phys. Lett.* **2011**, *512*, 237.
- (23) Beqa, L.; Fan, Z.; Singh, A. K.; Senapati, D.; Ray, P. C. *ACS Appl. Mater. Interfaces* **2011**, *3*, 3316.
- (24) Hu, M.; Chen, J.; Li, Z. Y.; Au, L.; Hartland, G. V.; Li, X.; Marquez, M.; Xia, Y. *Chem. Soc. Rev.* **2006**, *35*, 1084.
- (25) Huang, X.; El-Sayed, I. H.; Qian, W.; El-Sayed, M. A. *J. Am. Chem. Soc.* **2006**, *128*, 2115.
- (26) Huang, X.; Jain, P.; El-Sayed, I.; El-Sayed, M. *Laser Med. Sci.* **2008**, *23*, 217.
- (27) Lee, K. J.; Nallathamby, P. D.; Browning, L. M.; Osgood, C. J.; Xu, X.-H. N. *ACS Nano* **2007**, *1*, 133.
- (28) Shukla, R.; Bansal, V.; Chaudhary, M.; Basu, A.; Bhonde, R. R.; Sastry, M. *Langmuir* **2005**, *21*, 10644.
- (29) Greulich, C.; Kittler, S.; Epple, M.; Muhr, G.; Köller, M. L. *Arch. Surg.* **2009**, *394*, 495.
- (30) Robinson, J. T.; Welsher, K.; Tabakman, S. M.; Sherlock, S. P.; Wang, H.; Luong, R.; Dai, H. *Nano Res.* **2010**, *3*, 779.
- (31) Moon, H. K.; Lee, S. H.; Choi, H. C. *ACS Nano* **2009**, *3*, 3707.
- (32) Chandrasekar, G.; Mougin, K.; Haidara, H.; Vidal, L.; Gnecco, E. *Appl. Surf. Sci.* **2011**, *257*, 4175.
- (33) Ma, Z.; Tian, L.; Wang, T.; Wang, C. *Anal. Chim. Acta* **2010**, *673*, 179.
- (34) Zheng, M.; Jagota, A.; Strano, M. S.; Santos, A. P.; Barone, P.; Chou, S. G.; Diner, B. A.; Dresselhaus, M. S.; Mclean, R. S.; Onoa, G. B.; Samsonidze, G. G.; Semke, E. D.; Usrey, M.; Walls, D. J. *Science* **2003**, *302*, 1545.
- (35) Kam, N. W. S.; O'Connell, M.; Wisdom, J. A.; Dai, H. *Proc. Natl. Acad. Sci. U.S.A.* **2005**, *102*, 11600.
- (36) Tu, X.; Zheng, M. *Nano Res.* **2008**, *1*, 185.
- (37) Zheng, M.; Jagota, A.; Semke, E. D.; Diner, B. A.; McLean, R. S.; Lustig, S. R.; Richardson, R. E.; Tassi, N. G. *Nat. Mater.* **2003**, *2*, 338.
- (38) Oliveira, S.; van Bergen en Henegouwen, P. M.; Storm, G.; Schiffelers, R. M. *Expert Opin. Biol. Ther.* **2006**, *6*, 605.
- (39) Zhang, H.; Li, Y.; Ivanov, I. A.; Qu, Y.; Huang, Y.; Duan, X. *Angew. Chem., Int. Ed.* **2010**, *122*, 2927.
- (40) Kim, J.-H.; Bryan, W. W.; Randall Lee, T. *Langmuir* **2008**, *24*, 11147.
- (41) Cheng, L.; Yang, K.; Li, Y.; Chen, J.; Wang, C.; Shao, M.; Lee, S.-T.; Liu, Z. *Angew. Chem., Int. Ed.* **2011**, *123*, 7523.
- (42) Prencipe, G.; Tabakman, S. M.; Welsher, K.; Liu, Z.; Goodwin, A. P.; Zhang, L.; Henry, J.; Dai, H. *J. Am. Chem. Soc.* **2009**, *131*, 4783.
- (43) Wang, C.; Cheng, L.; Liu, Z. *Biomaterials* **2011**, *32*, 1110.
- (44) Nikoobakht, B.; El-Sayed, M. A. *Chem. Mater.* **2003**, *15*, 1957.